ChemComm

COMMUNICATION

View Article Online
View Journal | View Issue

Cite this: *Chem. Commun.*, 2025, **61**, 16958

Received 30th July 2025,
Accepted 26th September 2025

DOI: 10.1039/d5cc04346h

rsc.li/chemcomm

Linkage-dependent nano-conductivity of free-standing covalent organic membranes

Adithyan Puthukkudi,[ab] Subrat Rout,[ce] Amjath Nihal Thiruthimmal,[ab] Om Prakash Swain,[ab] Biplab K. Patra *[ce] and Bishnu P. Biswal *[abd]

Free-standing covalent organic membranes (COMs) with β-keto-enamine (TAPA-Tp), imine (TAPA-DTP), and vinylene (NTB-PDAN) linkages were interfacially fabricated, and their linkage-dependent nano-conductivity was probed using conductive atomic force microscopy (CAFM). The COMs exhibited excellent electrical continuity, with NTB-PDAN (15.78 pA) demonstrating superior nano-conductivity over TAPA-DTP (0.56 pA) and TAPA-Tp (0.42 pA).

Over the past few decades, membrane science and technology have undergone significant evolution, transitioning from a niche research area into a foundational pillar of modern materials science. Today, millions of square meters of membranes are produced annually, reflecting their broad applicability.[1] Although initially developed for separation[2–4] and ion transport,[5,6] now the membranes have expanded their functional scope to include roles in sensing,[7,8] energy storage,[9,10] and (opto)electronics.[11,12] The advent of flexible electronics has marked a significant paradigm shift in material science, emphasizing the importance of both mechanical robustness and electrical conductivity. In this context, COMs have garnered considerable attention owing to their intrinsic flexibility, incorporation of light elements, tunable functionality, and relatively low toxicity. While notable advancements have been achieved in the synthesis, structural design, and evaluation of properties at the macroscale of these membranes, critical insights at the nanoscale level remain limited. Echoing Richard Feynman's vision that "there is plenty of room at the bottom," Banerjee *et al.* conducted a seminal investigation into the nanoscale mechanical characteristics and morphology-dependent behavior of covalent organic framework thin films (Scheme 1a), highlighting the potential of such studies in advancing membrane performance.[13] However, until now, the nanoscale conductivity of covalent organic membranes (COMs) remains unexplored, despite its critical relevance for the rational design and integration of membrane-based electronic devices.

CAFM serves as a powerful tool for probing nano-conductivity, while simultaneously capturing surface topography, which is one of the main advantages as compared to other nanoelectronic techniques.[14] A typical CAFM setup comprises a conductive cantilever and probe, integrated with a laser and photodiode system to acquire both current mapping and topographical data. This nanoscale approach enables the

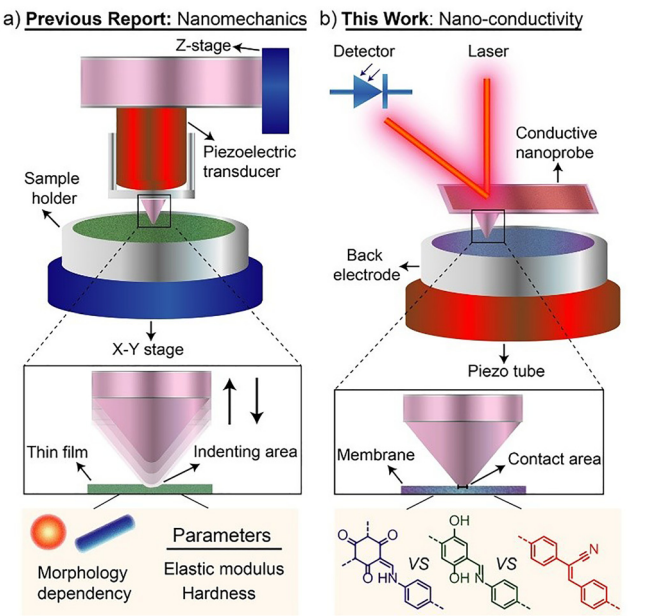

Scheme 1 Schematic representation of (a) the nanoindentation study using a triboindenter and (b) the nano-conductivity study using CAFM.

[a] *School of Chemical Sciences, National Institute of Science Education and Research Bhubaneswar, Jatni, Khurda, Odisha, 752050, India. E-mail: bp.biswal@niser.ac.in*
[b] *Homi Bhabha National Institute, Training School Complex, Anushakti Nagar, Mumbai, 400094, India*
[c] *Materials Chemistry & Interfacial Engineering Department, CSIR-Institute of Minerals and Materials Technology, Bhubaneswar, Odisha 751013, India. E-mail: bkpatra.immt@csir.res.in*
[d] *Centre for Interdisciplinary Sciences, National Institute of Science Education and Research Bhubaneswar, Jatni, Khurda, Odisha, 752050, India*
[e] *Academy of Scientific and Innovative Research (AcSIR), Ghaziabad 201002, India*

elucidation of distinct regions present in the system and their contribution towards the conductivity. In this study, we have judiciously fabricated COMs featuring distinct and well-established linkages [β-ketoenamine (TAPA-Tp), imine (TAPA-DTP), and vinylene (NTB-PDAN)] and systematically investigated the influence of linkage chemistry on nano-conductivity using CAFM (Scheme 1b). The COMs exhibited a linear surface current distribution with minimal deviation from average values, indicating uniform charge transport. Notably, the vinylene-linked NTB-PDAN membrane outperformed its counterparts by demonstrating a superior nano-conductivity of 15.78 pA. The insights of this study underscore the potential of designing COMs in advancing next-generation electronics, paving the way for further exploration of structure–property relationships and device-level integration.

Herein, we have adopted the interfacial polymerization technique to fabricate β-ketoenamine (TAPA-Tp), imine (TAPA-DTP), and vinylene-linked (NTB-PDAN) membranes [Fig. 1a(i)–c(i) and d]. TAPA-Tp and TAPA-DTP membranes were synthesized using a three-layer interfacial setup, wherein the bottom dichloromethane (DCM) layer contained the aldehyde monomer—either 2,4,6-trihydroxybenzene-1,3,5-tricarbaldehyde or 2,5-dihydroxyterephthalaldehyde—separated by an intermediate water layer from the top aqueous layer containing amine monomer, 4,4′,4″-triaminotriphenylamine. In contrast, the vinylene-linked NTB-PDAN membrane was fabricated using a two-layer interfacial approach, involving a bottom aqueous layer with KOH and a top organic layer [1,4-dioxane/cyclohexane (Cy)] comprising 4,4′,4″-trinitrotriphenylamine and *p*-phenylenediacetonitrile. The detailed fabrication protocol is provided in the SI (Section S1). The resulting membranes exhibited mechanical integrity with free-standing and flexible characteristics, as confirmed by digital images (Fig. 1d and Fig. S1–S3, SI).

For gaining insights into the surface morphology of the membranes, scanning electron microscopy (SEM) was employed. The SEM images revealed that the membranes possessed a crack-free and continuous surface on the scale of analysis, which is also confirmed by the optical microscopy [Fig. 1a(ii)–c(ii)]. Moreover, a close inspection revealed that the TAPA-DTP and NTB-PDAN membranes consist of microcrystallites having sphere-like morphology. In contrast, the TAPA-Tp membranes are made up of tubular-shaped crystallites (Fig. S4, SI). In line with this inference, we have measured thickness multiple times, and the average thickness is found to be 33, 26, and 44 μm for TAPA-DTP, TAPA-Tp and NTB-PDAN, respectively ([Fig. 1a(iii)–c(iii)] and Fig. S4, SI).

The chemical structures of the fabricated membranes were analyzed using Fourier transform infrared (FT-IR) spectroscopy and solid-state ^{13}C cross-polarisation magic angle spinning nuclear magnetic resonance (^{13}C CP-MAS NMR) spectroscopy (Fig. S5–S10, SI). Comparative analysis of the FT-IR spectra of the membranes with their corresponding monomers provided insights into the extent of monomer consumption. In the case of TAPA-DTP and TAPA-Tp membranes, the complete disappearance of the N–H stretching vibrations at ~3404 and ~3334 cm^{-1} confirmed the effective consumption of the amine monomers. The appearance of a C=N stretching vibration at 1607 cm^{-1}, along with a resonance at 162 ppm in the ^{13}C CP-MAS NMR spectrum, substantiated the formation of Schiff-base linkages in the TAPA-DTP membrane. For the TAPA-Tp

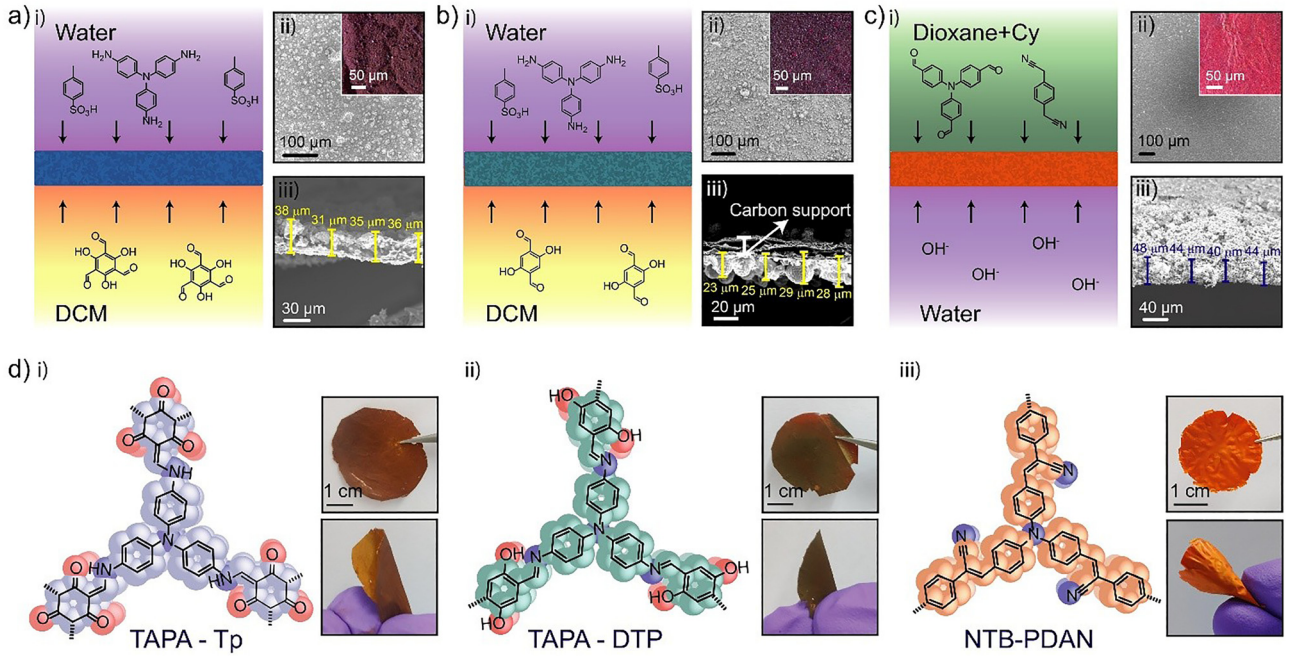

Fig. 1 Schematic representation of the fabrication (i) along with scanning electron microscopy (SEM) images of the surface (ii) and cross-section (iii) of (a) TAPA-Tp, (b) TAPA-DTP and (c) NTB-PDAN membranes (inset: optical microscopy images); (d) representative model and digital images of (i) TAPA-Tp, (ii) TAPA-DTP and (iii) NTB-PDAN membranes.

COM, the presence of characteristic vibrational bands at 1604 cm^{-1} (C═O) and 1578 cm^{-1} (C═C) in the FT-IR spectrum, along with NMR resonances at approximately 185 ppm and 108 ppm, confirmed the successful formation of β-ketoenamine linkages. Similarly, the FT-IR bands observed at 1584 cm^{-1} (C═C) and 2210 cm^{-1} (C≡N), together with the corresponding ^{13}C NMR peaks at ∼110 ppm and ∼120 ppm, provided strong evidence for the Knoevenagel condensation reaction in the NTB-PDAN COM. Additionally, the presence of C═O stretching bands at 1659 cm^{-1} and 1684 cm^{-1} in the TAPA-DTP and NTB-PDAN membranes, respectively, may be attributed to peripheral carbonyl groups and/or solvent-induced fragmentation.[15] We have also investigated the crystallinity using X-ray diffraction, and the COMs are found to be amorphous (Fig. S11, SI).

While considering application aspects, the mechanical properties play a pivotal role. We employed force microscopy studies to understand the mechanical properties of the membranes (Fig. S12, SI). Among the three, the NTB-PDAN COM exhibited the lowest Young's modulus (Y) value (∼14 MPa), which indicates its soft nature. The TAPA-Tp (Y = ∼183 MPa) achieved the highest stiffness by surpassing the TAPA-DTP COM (Y = ∼32 MPa). Furthermore, the chemical stability of the COMs was evaluated (Fig. S13–S21). The TAPA-Tp and NTB-PDAN COMs retained their structural integrity in organic solvents as well as under stronger acidic and basic conditions, while TAPA-DTP only retained its integrity in organic solvents and mild acidic conditions. Thermal gravimetric analysis revealed that the NTB-PDAN membrane exhibited the highest resistance to thermal degradation, maintaining stability up to 400 °C. In comparison, TAPA-Tp showed moderate thermal stability up to 320 °C, while TAPA-DTP (300 °C) displayed a comparatively lower stability (Fig. S22, SI).

The electronic band structure of the fabricated membranes was investigated using UV-Visible diffuse reflectance spectroscopy (UV-Vis DRS) (Fig. S23, SI). The UV-Vis DRS spectra revealed broad absorption features with multiple maxima. The optical band gaps were estimated by applying the Kubelka–Munk function to the reflectance data. Although the band gap values were closer, the TAPA-DTP exhibited a relatively lower band gap of 1.89 eV, while TAPA-Tp and NTB-PDAN showed band gaps of 2.12 eV and 2.16 eV, respectively. These band gap values reveal the semiconducting nature of the membranes.

Motivated by the inherent semiconducting nature of the COMs, we employed CAFM to investigate their nanoscale electrical conductivity under an ideal applied bias of 2 V (Fig. S24, SI).[14] This technique enabled simultaneous acquisition of current mapping and surface topography across all three membrane systems, facilitating a detailed analysis of the influence of linkage chemistry on local conductivity and structure-dependent charge transport pathways in COMs.

Fig. 2a–c shows the CAFM topographic images of TAPA-Tp, TAPA-DTP, and NTB-PDAN, revealing distinct morphological changes that may be attributed to structural linkages and reaction conditions. Although the COMs exhibit differences in micro-morphology, the CAFM technique provides localized conductivity mapping at the nanoscale, which is minimally influenced by the presence of microscale crystallites. TAPA-Tp exhibits a heterogeneous surface characterized by prominent granular elevations dispersed across a relatively flat background. These non-uniformly distributed granules appear as large, semi-spherical aggregates, resulting in a rougher texture. TAPA-DTP displays a comparatively smoother surface, with fewer spherical granules scattered irregularly across the membrane, suggesting less roughness relative to TAPA-Tp. Among the three membranes, NTB-PDAN presents good morphological uniformity with minimal presence of spherical granules. Fig. 2d–f display the corresponding current maps of TAPA-Tp, TAPA-DTP, and NTB-PDAN, at 2 V applied bias. We have also calculated the current histograms from the current maps to get insights into the distribution of the current across the COMs (Fig. 2g). The average surface current is found to be

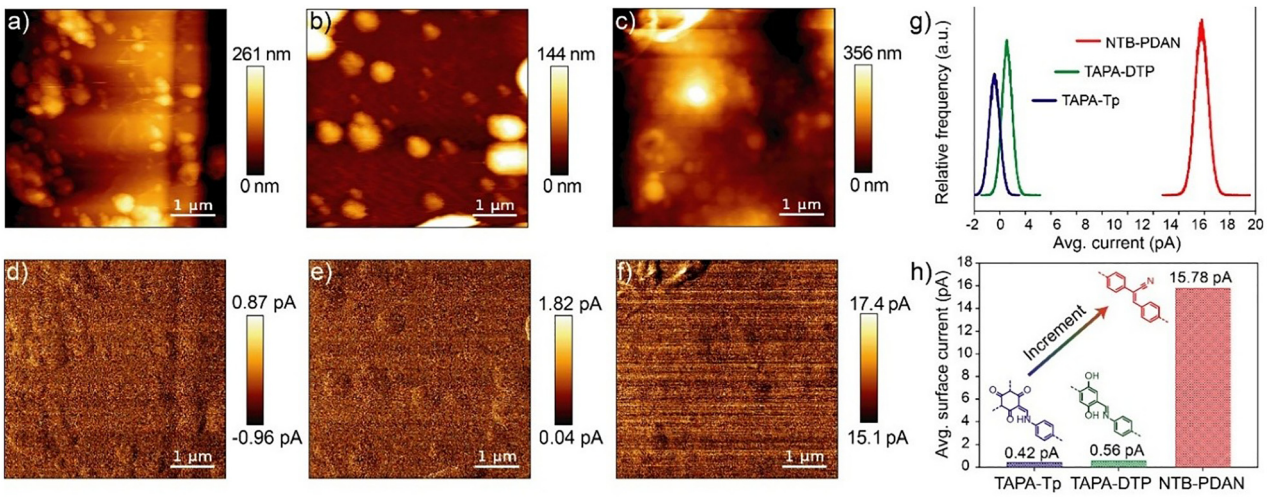

Fig. 2 (a)–(c) Represent the CAFM topographic images of TAPA-Tp, TAPA-DTP, and NTB-PDAN COMs, respectively, while (d)–(f) display their corresponding CAFM current maps at 2 V applied bias on a 5 μm × 5 μm area, and (g) shows the combined current histograms for the COMs, while (h) compares their average surface currents at an applied bias of 2 V.

15.78 pA for NTB-PDAN, while the value successively decreases to 0.56 pA and 0.42 pA in the case of TAPA-DTP and TAPA-TP, respectively (Fig. 2h).

While considering the band gap values, the obtained conductivity results are particularly interesting. However, electrical conductivity is not solely governed by the band gap, but is also equally influenced by the charge carrier diffusion coefficient (D), which is significantly dependent on the type of linkage and the surrounding chemical environment. The situation of D approaching zero imparts insulating behavior to materials, regardless of their band gap, known as the ''Anderson insulator''.[16] Among the studied systems, TAPA-DTP contains imine linkages and exhibits a relatively higher degree of conjugation compared to TAPA-Tp, which features β-ketoenamine linkages. In contrast, NTB-PDAN lacks highly electronegative nitrogen atoms in the linkage, potentially enhancing charge delocalization. However, the significantly lower nanoscale conductivity observed for TAPA-DTP cannot be solely attributed to the linkage structure or presence of nitrogen. The reduction is likely due to hydrogen bonding interactions between hydroxyl groups and the imine nitrogen, which impart a partial positive character to the nitrogen atoms and restrict electron flow.[17] However, a quantitative evaluation of the charge carrier diffusion coefficient remains inherently challenging, since the amorphous nature of the COMs prevents the acquisition of well-defined structural information, which is essential for such analysis.

Furthermore, we analysed the current mapping to understand the distinct regions present within the COMs. The brighter regions in the current map show maximum localized current density, while the darker regions are responsible for lower current density. However, across all the organic membranes, a linear current variation is observed with slight fluctuation centered around their respective average surface current. Despite the height variations arising from the granular structures, the current maintains a relatively stable baseline, indicating good electrical continuity and reproducibility throughout the surfaces for all the organic membranes (Fig. S25 and S26, SI). Although NTB-PDAN exhibits superior nanoscale electrical conductivity under applied bias compared to the other two membranes, the maximum value of current lies in the picoampere range, which suggests that the charge transport of these COMs is moderate, which may be attributed to localized charge carriers and limited long-range electronic delocalization. Overall, these moderate conductivity and uniform charge transport pathways are essential for device integration in low-power electronic applications.[18,19]

In summary, we interfacially fabricated β-ketoenamine, imine, and vinylene-linked free-standing COMs and studied the influence of linkage on the nano-conductivity using CAFM. On analysis, the vinylene-linked NTB-PDAN membrane exhibited excellent nano-conductivity (15.78 pA) and outperformed its counterparts, which establishes the correlation between linkage chemistry and nanoscale charge transport. These insights open new avenues for engineering conductive COMs toward future integration in flexible electronics.

This work is financially supported by the DST-INSPIRE Faculty Grant (IFA19-MS161), Govt. of India. B. P. B. acknowledges the Max Planck Society for support under the Max Planck India Partner Group project. B. P. B. thanks the DAE, Govt. of India, and NISER Bhubaneswar for financial and infrastructural support. B. K. P. wants to acknowledge the CSPS24/RDSF/IHP-000008 seed grant, GAP-341 (SERB), for providing partial financial support. S. R. acknowledges UGC for the fellowships.

Conflicts of interest

There are no conflicts to declare.

Data availability

The data supporting this article have been included as part of the supplementary information (SI). Supplementary information is available. See DOI: **https://doi.org/10.1039/d5cc04346h**.

Notes and references

1 R. W. Baker, *Membrane technology and applications*, John Wiley & Sons, Hoboken, New Jersey, 2023.
2 Y. Wang, N. Alaslai, B. Ghanem, X. Ma, X. Hu, M. Balcik, Q. Liu, M. A. Abdulhamid, Y. Han, M. Eddaoudi and I. Pinnau, *Adv. Mater.*, 2024, **36**, 2406076.
3 G. Liu, A. Cadiau, Y. Liu, K. Adil, V. Chernikova, I. D. Carja, Y. Belmabkhout, M. Karunakaran, O. Shekhah, C. Zhang, A. K. Itta, S. Yi, M. Eddaoudi and W. J. Koros, *Angew. Chem., Int. Ed.*, 2018, **130**, 15027–15032.
4 H. Yang, H. Zhang, C. Kang, C. Ji, D. Shi and D. Zhao, *Sci. Adv.*, 2024, **10**, eads0260.
5 X. Liu, X. Li, X. Chu, B. Zhang, J. Zhang, M. Hambsch, S. C. Mannsfeld, M. Borrelli, M. Löffler, D. Pohl, Y. Liu, Z. Zhang and X. Feng, *Adv. Mater.*, 2024, **36**, 2310791.
6 X. Liu, Z. Wang, Q. Zhang, D. Lei, X. Li, Z. Zhang and X. Feng, *Angew. Chem., Int. Ed.*, 2024, **63**, e202409349.
7 P. Zhang, S. Chen, C. Zhu, L. Hou, W. Xian, X. Zuo, Q. Zhang, L. Zhang, S. Ma and Q. Sun, *Nat. Commun.*, 2021, **12**, 1844.
8 H. Stapf, F. Selbmann, Y. Joseph and P. Rahimi, *ACS Appl. Electron. Mater.*, 2024, **6**, 2120–2133.
9 J. Hu, X. Tang, Q. Dai, Z. Liu, H. Zhang, A. Zheng, Z. Yuan and X. Li, *Nat. Commun.*, 2021, **12**, 3409.
10 H. S. Sasmal, H. B. Aiyappa, S. N. Bhange, S. Karak, A. Halder, S. Kurungot and R. Banerjee, *Angew. Chem., Int. Ed.*, 2018, **130**, 11060–11064.
11 Y. Lu, S. Krishna, C.-H. Liao, Z. Yang, M. Kumar, Z. Liu, X. Tang, N. Xiao, M. B. Hassine, S. T. Thoroddsen and X. Li, *ACS Appl. Mater. Interfaces*, 2022, **14**, 47922–47930.
12 A. Puthukkudi, S. Nath, P. Shee, A. Dutta, C. V. Rajput, S. Bommakanti, J. Mohapatra, M. Samal, S. Anwar, S. Pal and B. P. Biswal, *Adv. Mater.*, 2024, **36**, 2312960.
13 K. Dey, S. Bhunia, H. S. Sasmal, C. M. Reddy and R. Banerjee, *J. Am. Chem. Soc.*, 2021, **143**, 955–963.
14 M. Lanza, *Conductive atomic force microscopy: applications in nanomaterials*, John Wiley & Sons, Hoboken, New Jersey, 2017.
15 A. K. Mohammed, A. A. Al Khoori, M. A. Addicoat, S. Varghese, I. Othman, M. A. Jaoude, K. Polychronopoulou, M. Baias, M. A. Haija and D. Shetty, *Angew. Chem., Int. Ed.*, 2022, **134**, e202200905.
16 S. M. Girvin and K. Yang, *Modern condensed matter physics*, Cambridge University Press, Cambridge, 2019.
17 S. Kandambeth, V. Venkatesh, D. B. Shinde, S. Kumari, A. Halder, S. Verma and R. Banerjee, *Nat. Commun.*, 2015, **6**, 6786.
18 Q. Liu, Q. Li, Y. Li, T. Su, B. Hou, Y. Zhao and Y. Xu, *Angew. Chem., Int. Ed.*, 2025, **64**, e202502536.
19 J.-X. Jiang, A. Trewin, D. J. Adams and A. I. Cooper, *Chem. Sci.*, 2011, **2**, 1777–1781.